Distribution Agreement

In presenting this thesis as a partial fulfillment of the requirements for a degree from Emory University, I hereby grant to Emory University and its agents the non-exclusive license to archive, make accessible, and display my thesis in whole or in part in all forms of media, now or hereafter now, including display on the World Wide Web. I understand that I may select some access restrictions as part of the online submission of this thesis. I retain all ownership rights to the copyright of the thesis. I also retain the right to use in future works (such as articles or books) all or part of this thesis.

Ashwin Ragupathi April 3, 2018

Size Dependence of Gold Nanoparticles – How Site-Specific Conjugation to Dihydrofolate Reductase Alters Characteristics

by

Ashwin Ragupathi

R. Brian Dyer

Adviser

Department of Chemistry

R. Brian Dyer

Adviser

Jeremy Weaver

Committee Member

Periasamy Selvaraj

Committee Member

Rachel Kozlowski

Committee Member

2018

Size Dependence of Gold Nanoparticles – How Site-Specific Conjugation to Dihydrofolate Reductase Alters Characteristics

By
Ashwin Ragupathi

R. Brian Dyer
Adviser

An abstract of
a thesis submitted to the Faculty of Emory College of Arts and Sciences
of Emory University in partial fulfillment
of the requirements of the degree of
Bachelor of Sciences with Honors

Department of Chemistry

2018

Abstract
Size Dependence of Gold Nanoparticles – How Site-Specific Conjugation to Dihydrofolate Reductase Alters Characteristics
By Ashwin Ragupathi

Using the enzyme Dihydrofolate reductase (DHFR) and 5 nm, 15 nm and 30 nm AuNPs, both the effect of site-specific binding and the effect of AuNP size on the activity of the enzyme can be investigated. In order to allow AuNPs to conjugate to different locations on DHFR, the two intrinsic cysteines were replaced with non-thiol amino acids, and a single cysteine or His-Tag was placed into desired attachment sites.

The characterization of the free enzymes and conjugates, as well as the stability and preparation of both was investigated. The free mutants and wild type DHFR were prepared using TEV cleavage, and demonstrated a similar enzyme activity of about 30 turnovers s^{-1} and activation energies of approximately 75-79 kJ/mol. Once conjugates were formed, Tween 20 was used to stabilize them. SDS-PAGE showed that the DHFR mutants adequately conjugate with AuNPs and a novel fluorescence assay was developed to determine the concentration of protein bound to AuNPs. Ratios of conjugated enzyme to AuNP were also determined. UV/Vis analysis determined free AuNP had a SPR λ_{max} absorbance at 519 nm while conjugation red-shiftted the λ_{max} absorbance to 525 nm. Dynamic Light Scattering was used to determine that a monolayer of DHFR forms around the AuNP. Also, the activity of the conjugates mostly ranged from about 0.4 to 1.5 turnovers s^{-1}. Varying the sizes of the AuNP did not have much of an effect on the activity when compared to that of other conjugates. Also, these findings demonstrate that conjugation to AuNP greatly decreases the activity of DHFR, and that AuNP attachment affects the kinetics and dynamics of DHFR.

Size Dependence of Gold Nanoparticles – How Site-Specific Conjugation to Dihydrofolate Reductase Alters Characteristics

By

Ashwin Ragupathi

R. Brian Dyer

Adviser

A thesis submitted to the Faculty of Emory College of Arts and Sciences
of Emory University in partial fulfillment
of the requirements of the degree of
Bachelor of Sciences with Honors

Department of Chemistry

2018

Acknowledgements

I would like to thank my research adviser Dr. Brian Dyer for allowing me to work in his lab and pursue and honors thesis. The experience has allowed me to grow. Thank you for guiding me throughout the time I was an undergraduate in your lab.

Also, I would like to thank Dr. Jeremy Weaver and Dr. Periasamy Selvaraj for being my committee members. Thank you for allowing me to excel throughout as undergraduate at Emory University.

I would like to extend a huge thank you to Rachel Kozlowski for being my mentor and committee member. Without her, I would not have been able to complete this thesis and would not have been able to study site-specific gold nanoparticle attachments. Also, I would like to thank the rest of the Dyer Group for making my time in the lab enjoyable and helping me grow as a chemist.

I would also like to thank my friends and family for helping me get this far.

Table of Contents

List of Figures and Tables

Part I: Introduction to Gold Nanoparticles and Dihydrofolate Reductase

1.1 Introduction

1.1.1 Goals and Aims

Although enzyme and gold nanoparticle (AuNP) conjugation has been extensively studied, there is a lack of literature about how site-specific binding of AuNPs affect the overall activity of an enzyme. Using the enzyme dihydrofolate reductase (DHFR) and 5 nm, 15 nm and 30 nm AuNPs, both the effect of site-specific binding and the effect of AuNP size on the activity of the enzyme can be investigated. To allow AuNPs to conjugate to different locations on DHFR, the two intrinsic cysteines were replaced with non-thiol amino acids, and a single cysteine or His-Tag was placed into desired locations. With this investigation the following questions can be tackled: what effects does site specific conjugation of AuNPs have on enzymes, more specifically DHFR? How can mutant DHFR be prepared to allow for conjugation to AuNPs? How can AuNPs be prepared and conjugates be stabilized? What are the characteristics of the conjugates? To answer the aforementioned questions, it is necessary to characterize the mutants, make DHFR-AuNP conjugates and develop a method of maintaining conjugate stability. After these steps, characterization of the conjugates is imperative and this study is necessary. It was hypothesized that the larger the AuNP attached to the enzyme, the less activity the enzyme would have. It was also hypothesized that an attachment to a major catalytic loop, the FG loop, on the enzyme would decrease the activity of the enzyme more than that of any other attachment site. A third hypothesis was that attachment of an AuNP to a site furthest from the active site of an enzyme would have the greatest activity when compared to other conjugates.

1.1.2 The Gold Nanoparticle

Nanoparticles have been used extensively for modern biotechnological applications due to their dispersibility, surface area and ability to be utilized with various devices.[1] However, there is an extensive history of the use of metallic nanoparticles to produce art.[2,3] The Lycurgus cup, circa 4th century Rome, is an example of how gold and silver nanoparticles were used to create a dichromic effect, in which the glass reflects one color and transmits the light of another. The glass of Lycurgus's cup is green when viewing the glass from the outside but red when viewed with a light source on the inside. The dichromic effect is due to the varying sizes of the nanoparticles since metallic nanoparticles demonstrate different optical properties depending on their sizes.[3]

The use of AuNPs has diversified to include biotechnological advancements. During the 20th century, AuNPs started to be used for more scientific applications, including conjugation to attached enzymes for biocatalysts[4], biosensing[5], biofuels[6], disease diagnosis[7], and drug delivery[7]. Advancements in functionalization of AuNPs have led to an expansion of their potential in biomedical application, which has led to many *in vitro* and *in vivo* studies using AuNPs. Biodistribution *in vivo* studies in mice determined clearances and toxicities of various bioconjugates of AuNPs used for therapeutics and diagnostics. These AuNP conjugates tend to be deposited in the liver, spleen and other organs.[7] Furthermore, it was found that AuNPs with larger diameters tend to have a slower clearance rate *in vivo*,[7] making it imperative to study how varying sizes of AuNP effects the characteristics of bioconjugates *in vitro* and *in vivo*. The same study also tested conjugated to necrotic receptor proteins that would target cancer cells within mice. The conjugation of enzyme to the gold nanoparticles was important because it allowed for the tumor to be located on X-rays. However, these diagnostic techniques never reached clinical trials due to the slow clearance rates of AuNPs.[7]

Another unique characteristic of AuNPs is their surface plasmon resonance (SPR). SPR is an optical technique used to detect molecular reactions by measuring the resonant oscillations of conduction electrons at the interface of both negatively and positively charged material that is stimulated by incident light.[8,9] The SPR absorption of AuNPs varies depending on the size and shape of the AuNP and changes depending on the dielectric constants of the conjugating capping ligands.[9,10] With the change of SPR during conjugation of AuNPs and protein, it is interesting to investigate how SPR and other characteristics of AuNPs change when enzymes are bound. [10] Therefore, investigating size dependence of AuNPs when bound to enzymes is relevant.

1.1.3 What is DHFR?

Enzymes are biological catalysts that increase the rate of various biochemical reactions by reducing the required activation energy required. Reactions occur within the active site of an enzyme where the substrate, enzyme, and sometimes cofactor bind and allow for catalysis. Since these proteins allow reactions to occur fast enough to sustain life, there is a lot of interest in studying their dynamics and kinetics. DHFR is a heavily studied enzyme that catalyzes the reduction of 7,8-dihydrofolate (DHF) to 5,6,7,8-tetrahydrofolate (THF) by oxidizing nicotinamide dinucleotide phosphate (NAPDH) to $NADP^+$ (Figure 1.1 a,c),[11,12] (Figure 1.1c). The substrate reduction occurs with a hydride transfer from NADPH to DHF and a simultaneous proton transfer from the reaction environment.[11,12] This reaction is the major source of cellular THF.[11,12]

DHFR has three loops that are readily studied: FG loop, GH loop and Met20 loop. These loops have motions which allow for the aforementioned reaction to occur.[15] DHFR has three states, the open, the closed and occluded states. While in the open conformation, the enzyme is not bound to any cofactor or substrate. In the closed conformation, the Met20 loop covers the active site, preventing the substrate from leaving. In the occluded conformation, the loop moves to cover the

binding site of NADPH, sterically hindering this cofactor from binding to the active site (Figure 1.1b).[16-18] The largest conformational change occurs in the Met20 loop of DHFR while NADPH binds to its binding pocket.[18]

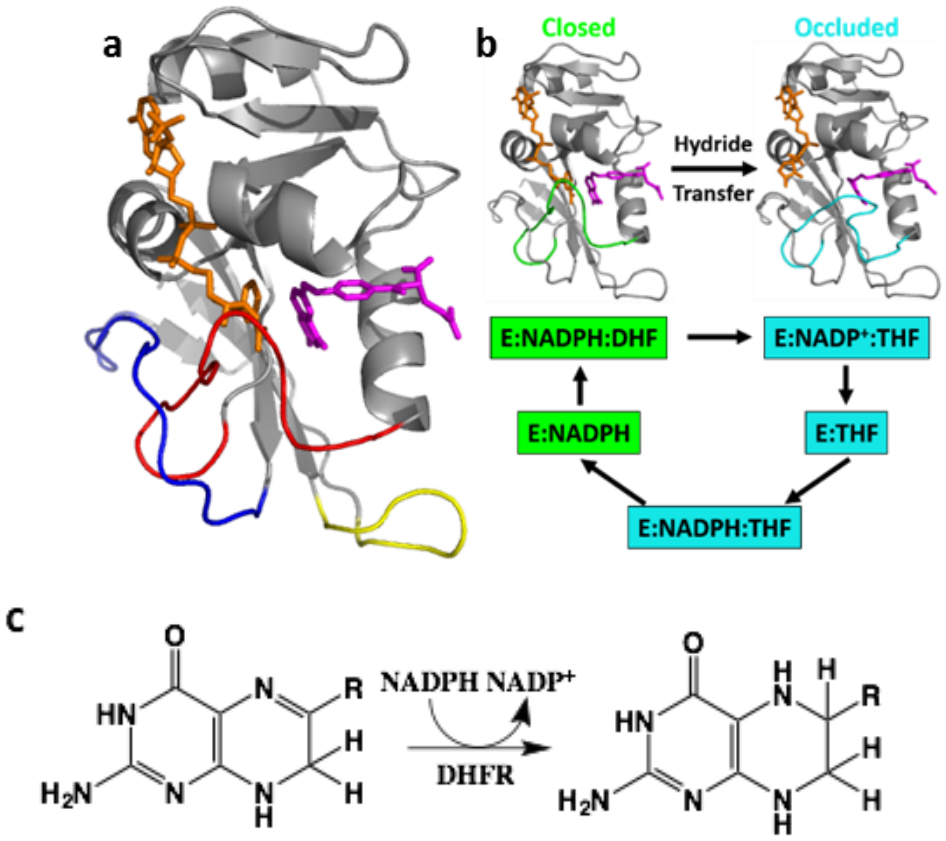

Figure 1.1: Structure and catalytic cycle of DHFR. **A:** Crystal structure of DHFR with cofactor NADPH (pink) and substrate DHF (orange). The red loop represents the Met20 loop. The blue is the FG loop. The yellow is the GH loop. PDB code: 1RX2. **B:** Catalytic cycle of DHFR including crystalized structures of close and occluded states of DHFR. Met20 loop in the closed state is represented in green, and is represented in blue when it is occluded. All intermediates in the closed conformation (PDB code: 1RX2) are in green and the intermediates in the occluded conformation (PDB code: 1RX7) are in blue. Reproduced from Reference 17. **C:** The reaction that occurs when DHF is converted to THF through the oxidation of the cofactor NADPH by the enzyme DHFR.

DHFR is an enzyme of interest due its use as a target for treatments since the enzyme is required to make THF, eventually used to make thymine,[11,12] which is excessively produced in rapidly proliferating cells.[19] A common inhibitor of DHFR used as a cancer treatment is methotrexate (MTX), which competitively binds in the substrate binding pocket. It was revealed

that MTX binds to two different conformations of the enzyme on the loops, and competitively inhibits the activity of the enzyme.[20] DHFR is also targeted in many Gram-positive bacterial diseases through Trimethoprim (TMP). TMP is an oral antibiotic drug that is used to competitively inhibit the DHFR in bacteria, which in turn eliminates bacterial infections. TMP is not used for cancer drugs because its affinity for bacterial DHFR is thousands of times greater than that of human DHFR, hence making it ideal to target bacterial infections.[21] It is biologically relevant to study the motions and kinetics of DHFR, since DHFR is greatly studied and utilized in modern medicine. This investigation utilizes *Escherichia coli* DHFR because it is approximately 1,000 times slower than human DHFR and has known loop motions that can be studied.[13-18]

1.1.4 Mutants of DHFR

To further investigate the dynamics of DHFR, site-specific surface attachments can be made to mutant strains of *E. coli* DHFR with AuNPs. In wild-type (WT) DHFR there are two intrinsic cysteines located at the 85th (C85) and 152nd (C152) positions, however both these cysteines not on areas of interest for this investigation. By mutating out these cysteines and replacing them with serine and alanine, while also replacing certain amino acids on locations of interest with cysteines, site-specific additions of AuNPs can be made through Au-S covalent bonds.[22,23]

Four different mutants were used to investigate how site-specific attachment affects characteristics and conjugation of DHFR with AuNPs: FG Loop Mutant, Alpha Helix Mutant, Distal Active Site Mutant and His-Tag Mutant. The FG Loop mutant has a mutation on the 120th position, E120C. E120 is adjacent to G121 on the FG loop, which is known to be central to catalysis.[24] The site-specific attachment of AuNPs to the FG loop allows for the investigation of interactions between AuNPs and the FG loop.

The Alpha Helix mutant has a mutation on the 101st position, E101C. E101 is on an inflexible alpha helix, but still near the active site of DHFR. Attachment of the AuNP on a location that does not move during catalysis serves as a control when comparing to the FG Loop Mutant attachment. The Distal Active Site mutant has a mutation on the 87th position, D87C. D87 is on an alpha helix further away from the active site than that of the other two single cysteine mutants. Attachment here will help determine if activity of AuNP conjugates from the FG Loop mutant and the Alpha Helix Mutant is due to the proximity of the attachment site to the active site of the enzymes (Figure 1.2). The His-Tag mutant has no cysteines, but a His-Tag is present. The AuNP will strongly associate with the His-Tag, which has a K_d of 1 - 5 nM.[25] This attachment site is far away from the active site in DHFR. The His-Tag Mutant also allows for the studying of a different surface attachment method from the other three mutants. The bond strength of Au-S bond is characterized as 418 kJ/mol[26] and the K_d of the Au-His-Tag association is approximately 1-5 nM,[27] allowing for a comparison between the two attachment methods. It is hypothesized the attachment to the FG loop would have the greatest effect on activity due to its involvement in catalysis when compared to conjugates with the other mutants and the Distal Active Site Mutant conjugates would have the greatest activity due to its distance from the active site.

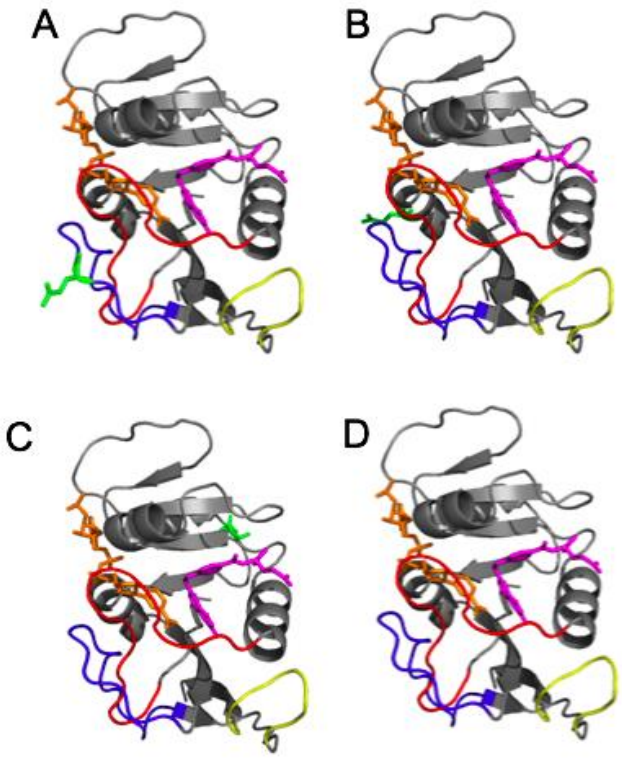

Figure 1.2: Structure of single cysteine mutants of DHFR. The flexible loops of the protein are colored: Red = Met20 loop, blue = FG loop, and yellow = GH loop. The green residues are mutated to a cysteine. PDB code: 1RX2. **a.** FG Loop mutant, where E120C cysteine is mutated on the FG Loop. **b.** Alpha Helix mutant, E101C cysteine is mutated on an alpha-helix. **c.** Distal Active Site mutant, D87C cysteine is mutated on an alpha-helix further from the active site than in the Alpha Helix Mutant. **d.** His-Tag mutant, where a hexahistidine tag is present, and all intrinsic cysteines were replaced. The hexahistidine tag was present at the C-terminus of the enzyme, and is not shown in the figure.

Part II: Preparation and Characterization of DHFR Mutants

2.1 Purpose

The purpose of this section of the thesis is to describe the preparation and characterization of the four mutants: FG Loop, Alpha Helix, Active Distal Site and His-Tag, prior to that of their conjugation to AuNP. Since these are novel mutants were developed, through genetic engineering *E. coli*, it is necessary to characterize them and compare to wild-type (WT) DHFR to ensure that the mutations do not heavily alter the structure and activity. Once it was determined that the mutations do not affect the free enzyme function, it was possible for further investigation and conjugation to AuNPs.

Characterization and preparation of DHFR mutants is substantiated by of the Tobacco Etch Virus (TEV) cleavage, activity of the free enzymes and Arrhenius information. The purpose of the TEV cleavage with the FG Loop, Alpha Helix and Distal Active Site Mutants is to remove the hexahistidine tag[28] that is present on the enzymes. The purpose of the His-Tag is to allow for purification of the enzyme, however, if left uncleaved, the two possible attachment sites (cysteine and His tag) to the AuNPs causes the DHFR-AuNP conjugates to aggregate and precipitate out of solution throughout the course of a day. The activity and Arrhenius information determine the turnovers and activation energy which allows for more comparable information among the WT and mutants.

2.2 Material and Methods

2.2.1 TEV Cleavage

The FG Loop, Alpha Helix and Distal Active Site Mutants originally contained a His-Tag which helped with purification of the enzymes. However, once the enzyme is purified, there is no need for the His-Tag, so it must be removed to leave one attachment site, the cysteine, for the

site-specific binding of AuNPs. TEV protease is used remove the His-Tag by recognizing the seven-amino-acid sequence Glu-Asn-Leu-Tyr-Phe-Gln-Gly and cleaves between Gln and Gly.

Initially, the uncleaved enzymes were stored in a -80°C freezer until the TEV cleavage was required. Once the enzymes were removed from the freezer, their concentrations were checked using a UV/Vis spectrometer, and were diluted to 250 μM using 50 mM sodium phosphate buffer. 20% by volume of TEV protease was added to the reaction solution and was left to react at 4°C for 24 to 48 hours.

After the reaction time was over, the solution was run through a Nickel-nitrilotriacetic acid (Ni-NTA) column. A Ni-NTA column was used to purify cleaved product because the His-Tags from uncleaved protein and TEV protease bind to it, while the cleaved protein flows through. To clean the resin, 150 mM imidazole buffer was run through the column to remove residual enzyme bound with His-Tag from the column. 20% ethanol was run thorough to store the resin.

The collected sample was then buffer exchanged in an Amicon ® Ultra – 15 Centrifugal filter, and was centrifuged six times at 5,000xg for 20 minutes each spin. The protein concentration was determined using the extinction coefficient of 3.11×10^4 M^{-1} cm^{-1} at 280 nm[29] with UV/Vis analysis with a Nanodrop 2000, then diluted to 50 μM enzyme concentration, and aliquoted into single use tubes. The samples were lyophilized and then stored at -20°C for up to three months.

To determine whether the TEV cleavage was successful, Sodium dodecyl sulfate polyacrylamide gel electrophoresis (SDS-PAGE) was run. To prepare the samples of protein, the samples were rehydrated with 1.42 mg/mL of Tris(2-carboxyethyl) phosphine hydrochloride (TCEP) and DI water and left to incubate at room temperature for approximately an hour, to prevent disulfide bonds from forming between the individual mutant enzymes.[30] A 50:50 ratio of protein and 2x Laemmli sample buffer was added. The samples were heated to boiling at 100°C

for 5 minutes, then immediately transferred to ice for 5 minutes. The samples were loaded into a polyacrylamide gel, placed in a Biorad Citerion™ Vertical Electrophoresis Cell with Tris/Glycine/SDS Buffer and then run at 200 V for 60 minutes. The gel was then stained with Coommassie blue and then destained.

2.2.2 Activity of Free Mutants

The lyophilized protein stocks were rehydrated with 1.42 mg/mL TCEP solution. The protein was diluted to 1 μM for the assay. 2.5 mM of DHF was prepared in a sealed amber vial and was put through a freeze, pump, thaw cycle 3 times to remove the excess oxygen in the vial, since DHF is easily oxidized. 5 mM of NADPH was prepared in a black Eppendorf tube because NADPH is light sensitive. NAPDH and DHF using molar absorptivity of 6220 cm^{-1} M^{-1} at 340 nm and 28,000 cm^{-1} M^{-1} at 282 nm.[29,31]

Before the reaction occurs, 10 μL of the 5 mM NADPH, 10 μL of the free protein and 960 μL of 50 mM sodium phosphate buffer was added to the cuvette and allowed to equilibrate for at 37°C in the Ocean Optics QPOD temperature controlled stage for 3 minutes. 20 μL of 50mM of DHF was added to the reaction mixture to initiate the reaction, and the reaction was monitored with an Ocean Optics QE65000 spectrometer via light from a Xenon lamp for 5 minutes. The absorbance at 340 nm was analyzed since NADPH depletion can be measured at this wavelength to determine the turnovers of the samples. A Perkin Elmer Lambda 35 UV/Vis Spectrometer was used to determine the exact concentrations of the free protein to account for pipetting error that could have slightly altered the concentration of the free protein samples throughout prep The turnovers were determined by adjusting for NAPDH and DHF using the integrated molar absorptivity of 11,800 cm^{-1} M^{-1} at 340 nm.

2.2.3 Arrhenius Information

Arrhenius information allows for the determination of the activation energies of enzymes and mutants. Samples were prepared in the same manner as mentioned in *2.2.2 Activity of Free Mutants*. Activity was measured using the same methods, but at the samples were run at 6 different temperatures: 22°C, 27°C, 32°C, 37°C, 42°C and 47°C. Using the turnovers at the different temperatures, Arrhenius plots were created by graphing ln(turnover) vs 1/T (in Kelvin). Using the Arrhenius equation, the activation energies of the free proteins were determined. The equation used was $k = Ae^{-\frac{E_a}{RT}}$, which was linearized to $lnk = -\frac{E_a}{R}\left(\frac{1}{T}\right) + lnA$, where *k* represents the rate constant, E_a represents the activation energy, *R* represents the gas constant, *T* represents temperature in Kelvin and A represents the frequency factor.[32] The slope of the aforementioned graph was determined to represent $-E_a/R$.

2.3 Results and Discussion

2.3.1 TEV Cleavage

TEV protease is used to cleave the His-Tag from the single cysteine mutants to leave a single binding site on the enzyme to bind to AuNPs. SDS-PAGE was used to determine the difference in mass of the cleaved and uncleaved protein and showed that cleaved protein had a lower molecular weight that the uncleaved protein (Figure 2.1). The mass difference represented the loss of the His-Tag which is about 1-2 kDa. Since the mass of the cleaved protein is less than that of the uncleaved protein, it travels further in the gel. Both the cleaved Alpha Helix and FG Loop mutants have a lower mass due to the removal of the His-Tag. The Distal Active Site mutant is not shown, but due to the similarities and characteristics to that of the other two mutants, it is fair to assume that it ideally runs through the gel in a similar manner as cleaved and uncleaved protein.

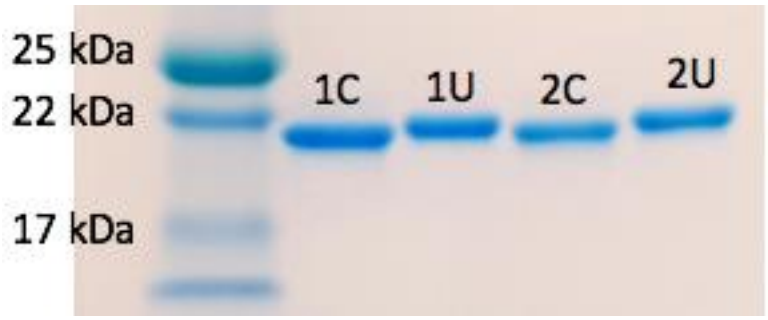

Figure 2.1. SDS-PAGE gel of cleaved FG Loop mutant (Lane 1C), uncleaved FG Loop mutant (Lane 1U), cleaved Alpha Helix mutant (Lane 2C) and cleaved Alpha Helix mutant (Lane 2U). The uncleaved protein is approximately 23 kDa and the cleaved protein runs about 22 kDa.

2.3.2 Activity of Free Mutants

The activity of the free mutants is important to determine that the mutations did not severely affect the activity of the enzymes. The FG Loop, Alpha Helix, Distal Active Site and His-Tag Mutant all had comparable activities to that of the WT DHFR (Table 2.1). The slightly lower turnover of the FG loop mutant may be due to FG loop motion being affected during catalysis, considering the FG Loop is one of the loops known to have the greatest motions during catalysis. Further, the E120C mutation on the FG Loop mutant is next to G121, which is known to be central to the enzyme's catalysis, which might affect catalysis.

Sample	Turnover (s^{-1})
WT DHFR	30.6 +/- 0.4
FG Loop Mutant	27.2 +/- 0.3
Alpha Helix Mutant	30.0 +/- 0.4
Distal Active Site Mutant	30.1 +/- 0.4
His-Tag Mutant	29.6 +/- 0.4

Table 2.1: Enzyme Turnovers for free WT DHFR, FG Loop, Alpha Helix, Distal Active Site and His-Tag Mutants. The errors represent standard deviations (n=3).

2.3.3 Arrhenius Information

Overall, these mutants were initially developed to determined how conjugation to different locations on the enzyme would affect heat flow into the protein. With possible heat flow experiments in the future, the following question arises: is change in activity due to bulk heating or heat flow? To answer any possible questions that may arise when heat flow experiments were done, Arrhenius plots were created to determine the activation energy of each of the mutants. The activation energy of WT DHFR and the mutants were similar and ranged from 74.9 – 79.4 kJ/mol. The data for the FG Loop Mutant is shown in Figure 2.2, and is similar to that of the other enzymes, so the temperature dependence activity for the other mutants and WT are not shown. Therefore, the mutations did not drastically affect the activation barriers.

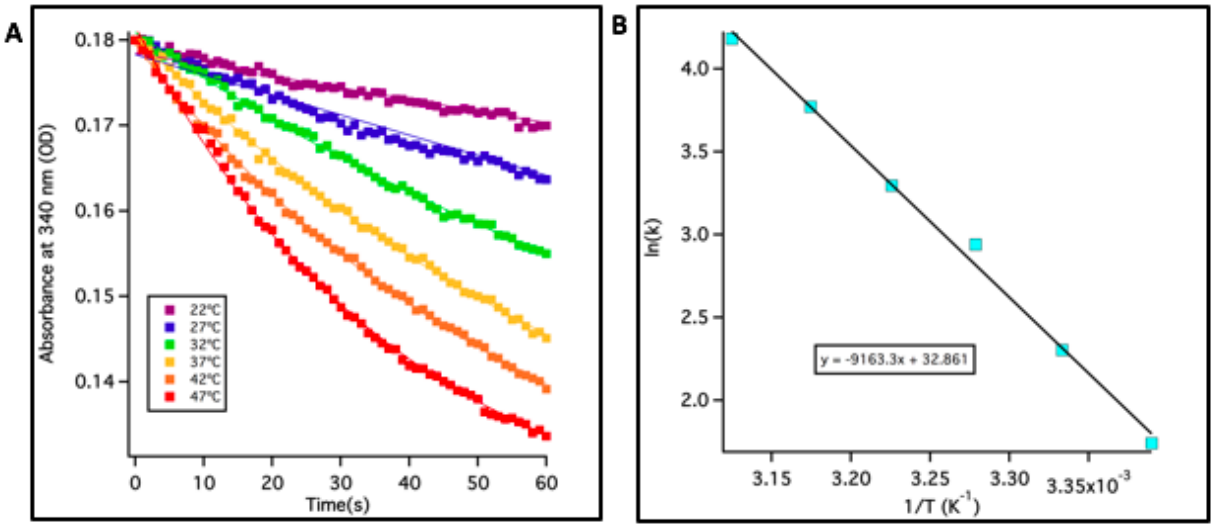

Figure 2.2. A: Activity of FG Loop Mutant at 22°C, 27°C, 32°C, 37°C, 42°C, 47°C **B:** Arrhenius plot used to determine the activation energy from the slope.

Sample	Activation Energy (kJ/mol)
WT DHFR	76.2 +/- 0.9
FG Loop Mutant	76.2 +/- 0.4
Alpha Helix Mutant	74.9 +/- 0.4
Distal Active Site Mutant	77.1 +/- 0.7
His-Tag Mutant	79.4 +/- 0.6

Table 2.2: Activation energy of free WT DHFR, FG Loop Alpha Helix, Distal Active Site and His-Tag Mutants. The errors show standard deviations (n=3)

Part III: Conjugation and Stability

3.1 Purpose

The purpose of this section is to describe the process of conjugating DHFR to AuNPs. 15 nm AuNPs were synthesized, and Transmission Electron Microscopy (TEM) and a UV/Vis spectrophotometry were used to ensure that the synthesized AuNPs were the anticipated size. The 5 nm and 30 nm AuNP were purchased from the company Nanocomposix, as they were not used nearly as much as the 15 nm AuNPs. This section also explores the effect of Tween 20 on the stability of the conjugates.

3.2 Materials and Methods

3.2.1 Synthesis of 15 nm AuNP

To synthesize 15 nm AuNP, the following protocol was adapted from reference 38. Initially, all the glassware was cleaned with aqua regia to dissolve any remaining gold, rinsed with filtered DI water, and dried in an oven at approximately 135°C. The glassware was then blown out with pressured air to speed up the cooling process, and a reflux apparatus was assembled with a two-neck round bottom flask, reflux condenser, Tygon tubing and a rubber septa. Teflon tape was used to ensure a perfect fit between the parts of the apparatus. 500 mL of 1 mM hydrogen tetrachloroaurate (III) trihydrate was prepared in a two neck round bottom flask, mixed using a stir bar, and brought to a boil under reflux. Once the gold solution was refluxing about 1 drip per second, the rubber septum was removed, 50 mL of 38.8 mM sodium citrate was quickly added to the refluxing solution, and the septum was immediately resealed. After 15 minutes, the heating was stopped, the flask was covered with aluminum foil, and the solution was cooled overnight at room temperature. The solution was filtered with a 0.45 μm acetate filter and stored in foil covered bottle at 4°C.

TEM was used to investigate the morphology of the synthesized AuNPs. TEM is a microscopy technique, where a beam of electrons transmitted through an ultra-thin specimen, in which it interacts and forms an image. The image is magnified and focused onto an imaging device to be detected by a sensor.[39] TEM is capable of obtaining images of high resolution AuNPs were diluted by a factor of 8, placed on a TEM grid, and allowed to evaporate/dry at room temperature. The voltage of the TEM used was 120 kV Once the images of the nanoparticles were captured, the program ImageJ was used to determine the size distribution of the AuNPs. To determine if the synthesized gold nanoparticles maintained similar optical properties to that of the Nanocomposix particles, UV/Vis spectra were acquired using a Nanodrop 2000.

3.2.2 Conjugation

During conjugate preparation, the single cysteine mutants will form Au-S bonds with AuNPs and the His tag mutant will strongly associate with the His-Tag. Each mutant was rehydrated with 1.42 mg/mL TCEP, to prevent disulfide bonds from forming,[30] and were left to incubate for at least an hour.

To make 5 nm conjugates, 400 μL of 2.40 nM 5 nm AuNPs were added to 30 μL of 50 mM free protein in a lo-bind Eppendorf tube and left to incubate overnight at 4°C to allow the conjugation to occur. The samples were centrifuged for 90 minutes at 13,200 rpm. The supernatant was removed, and the pellet was replenished with 0.005% Tween in 10 mM sodium phosphate buffer to wash the free protein from the pellet of DHFR-AuNP conjugates. After wash cycles, the pellet was stored in 0.005% Tween in 10 mM sodium phosphate buffer, and diluted accordingly.

To make 15 nm conjugates, the same methods to make 5 nm conjugates were made except centrifuging speeds and times were changed to 8000 rpm and 35 minutes for 800 μL of 7.88 nM 15 nm AuNP. To make 30 nm conjugates, the same methods to make 5 nm conjugates were made

except centrifuging speeds and times were changed to 8000 rpm and 10 minutes for 400 μL of 2.40 nM 15 nm AuNP.

3.2.3 Tween 20 and Free Protein

Samples were prepared in the same manner as the free proteins in *2.2.2 Activity of Free Mutants*, however the buffer with Tween 20 samples were at 0.005% Tween 20 by volume. Activity was run using the same methods. However, this data was not corrected by using a Perkin Elmer UV/Vis.

3.2.4 Tween 20 and Conjugates

Samples were prepared in the same manner as the conjugates in *3.2.2 Conjugation*

3.3 Results and Discussion

3.3.1 Characterization of 15 nm AuNPs

TEM microscopy was used to characterize the synthesized AuNPs (Figure 3.1). Visually, the nanoparticles are spherical in nature and roughly 15 nm in diameter. ImageJ was used to determine the size distribution of the synthesized AuNPs to be 14.1 ± 1.4 nm (Figure 3.2a). The UV/Vis verification determined that the synthesized AuNP have an absorbance peak at approximately 520 nm which is similar to that of the 15 nm AuNP from Nanocomposix (Figure 3.2b), meaning that the synthesis was successful.

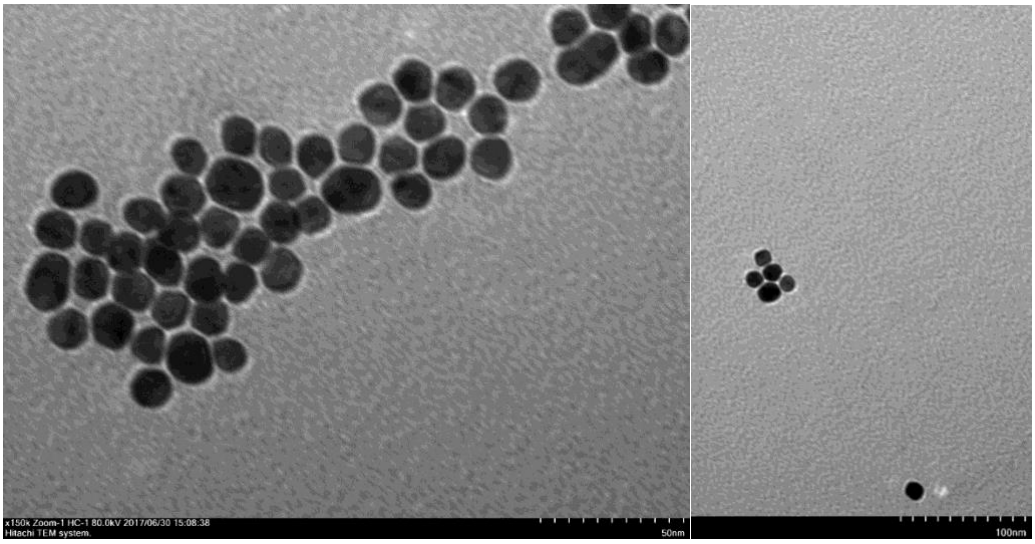

Figure 3.1: TEM image of synthesized 15 nm AuNPs. Reproduced from reference 17.

.

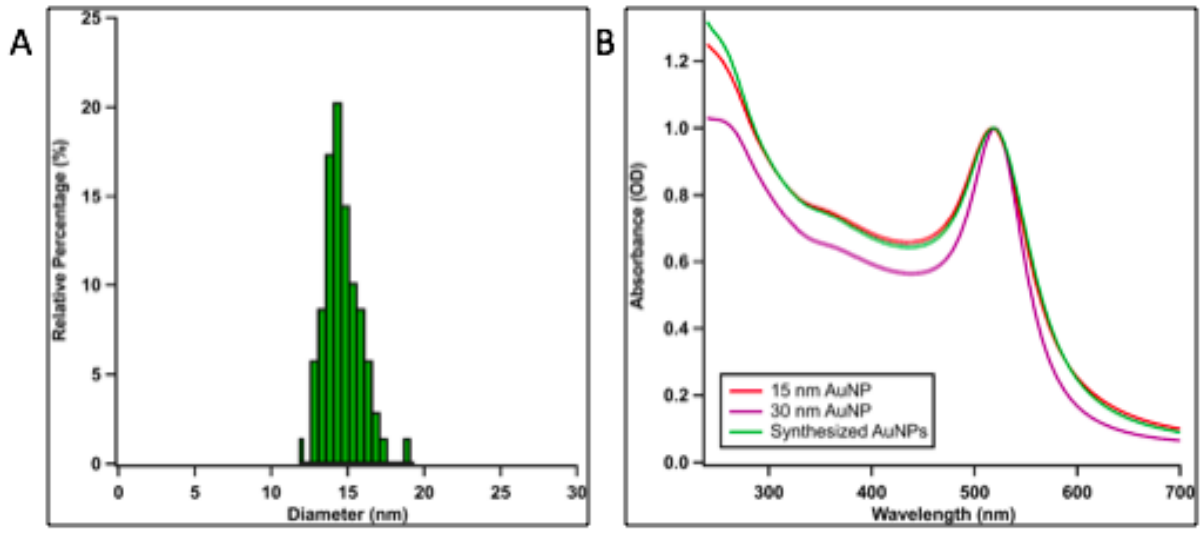

Figure 3.2 A: Size distribution of the synthesized AuNPs (left). **B:** UV/Vis spectra of both synthesized and Nanocomposix 15 nm AuNPs at 519 nm. Reproduced from reference 17.

3.3.2 Tween 20 and Free Protein

When introducing a new compound in the reaction sample such as Tween 20, it is ideal to check if it affects the activity of DHFR. To test the effect of Tween 20. the activity of the WT

and free mutants was run with and without 0.005% Tween 20 to make sure that the surfactant did not severely affect the enzymatic activity.

The FG Loop mutant, the Alpha Helix mutant, and the His-Tag mutant and WT DHFR are all comparable in the activity with and without Tween 20 as a stabilization agent since almost all of the values in Table 3.1 are within the error of the measurements.

Sample Type	**Turnover (s^{-1}) without Tween 20**	**Turnover (s^{-1}) with Tween 20**
WT DHFR	27.6 ± 0.5	30.6 ± 0.4
Alpha Helix Mutant	29 ± 2	28.2 ± 1.3
FG Loop Mutant	28 ± 2	27.2 ± 0.3
His-Tag Mutant	26 ± 2	27.6 ± 1.4

Table 3.1: Enzyme turnovers for the WT DHFR, Alpha Helix Mutant, FG Loop Mutant and His-Tag Mutant without and with Tween 20. (n=3)

3.3.3 Tween 20 and Conjugates

When it comes to stability, DHFR is stable in 50 mM sodium phosphate buffer, however, these conditions are not ideal for AuNPs. AuNP are stable in citrate buffer and salt-less solutions, and they will start to aggregate once placed in high salt containing buffer. To combat these non-ideal conditions, DHFR-AuNP conjugates were initially stored in 10 mM sodium phosphate buffer at 4°C. However, the activity of the conjugated DHFR would decrease rapidly. It was hypothesized that the reason this was happening was due to aggregation of the DHFR that were caused by empty regions of the AuNPs binding together. Previous studies have used Tween

20, thiol groups and other heterocyclic compounds to cap these empty regions.[33-35] For the purpose of these studies Tween 20 was used because Tween 20 has been used as a surfactant with DHFR in previous studies.[36,37]

FG Loop Mutant-15 nm AuNP and Alpha Helix Mutant-15 nm AuNP conjugates were used to test the effect of 0.005% Tween 20. Activity assays with these conjugates were run to determine the turnovers over multiple days to determine conjugate stability, and it was determined that the conjugates were active in Tween 20 for approximately 10 days when stored at 4°C. The activity of the covalently bound conjugates increases when the samples are stored in 0.005% Tween 20, which is indicative of stability (Table 3.2). The pipette tips used were all lo-bind; however, conjugates would stick to them. This problem would have consequences by altering the concentration, causing errors when determining concentration and activity. However, Tween 20 also solved this problem (Figure 3.3). Tween 20 prevented the loss of sample on lo-bind pipette tips, most likely due to the capping of empty spaces on the AuNPs with Tween 20 to prevent exposed AuNPs from attaching to pipette tips.

Sample Type	**Day 1 Turnover (s^{-1}) Without Tween 20**	**Day 1 Turnover (s^{-1}) With Tween 20**	**Day 7 Turnover (s^{-1}) With Tween 20**
FG Loop Mutant-15 nm AuNP	0.3 ± 0.2	0.83 ± 0.07	0.71± 0.08
Alpha Helix Mutant-15 nm AuNP	0.2 ± 0.1	0.71 ± 0.08	0.72± 0.04

Table 3.2: Enzyme turnovers for the DHFR-15 nm AuNP conjugates day one and seven days after conjugate preparation. (n=3)

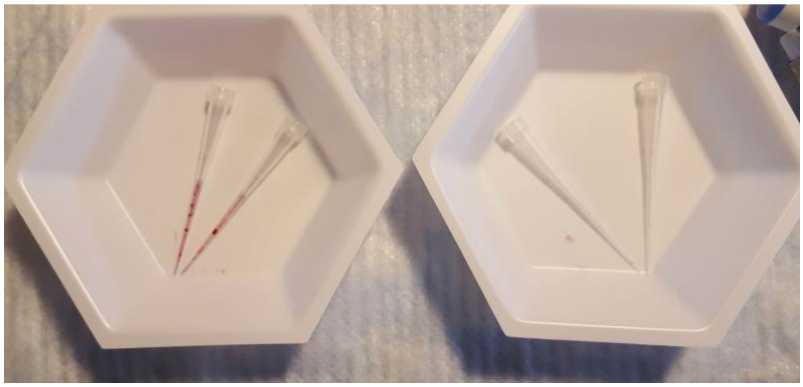

Figure 3.3 Pipette tips after transfer of DHFR-15 nm AuNP without Tween 20 (left) and with Tween 20 (right). The pink stain on the pipette tips is indicative of the conjugates sticking to the lo-bind pipette tips that were used throughout the experiments.

Part IV: DHFR-AuNP Conjugate Characterization

4.1 Purpose

Now we attempt to tackle the following question: what effects does site specific conjugation of AuNPs have on DHFR? To answer this question, characterization of the conjugates is imperative. This section includes an SDS-PAGE, Dynamic Light Scattering (DLS), a novel concentration determination assay, conjugate activity and a ratio of protein to AuNPs. In the long-term, this characterization protocol may be useful for the previously mentioned uses of enzyme-AuNP conjugation.

4.2 Materials and Methods

4.2.1 UV/Vis Verification

The conjugates were analyzed on the UV/vis to determine if the protein was bound to the AuNP. UV/Vis spectra were acquired using a Nanodrop 2000.

4.2.2 SDS-PAGE Gel

SDS-PAGE gels were run using the description in *2.2.1 TEV Cleavage*. The conjugates were run in a similar manner to that of the free protein.

4.2.3 Dynamic Light Scattering

Dynamic Light Scattering (DLS) is used to determine the size of a spherical molecule by measuring backscatter after a red laser interacts with the sample. To prepare for DLS, the conjugates were prepared using the protocol described in *3.2.2 Conjugation*, but were diluted by a factor of 10. Since the Particle Systems Nanoplus zeta/nano particle analyzer is unable to detect 5 nm conjugates due to their small size, it was not measured; however, information can be inferred from 15 nm and 30 nm conjugates. The samples were loaded in to a DLS microcuvette for this experiment.

4.2.4 Concentration Determination

To determine the concentration of protein on the AuNP, 32 μL of conjugates were dissolved in a 16 μL of a saturated potassium cyanide (KCN) solution. Once dissolved, 52 μL of 10 mM sodium phosphate buffer was added for a total volume of 100 μL. A standard curve was created using WT-DHFR such that 0.5 μM, 1 μM, 2 μM, 3 μM, 5 μM, and 10 μM were prepared in a similar manner as the conjugates, except 32 μL of the free protein was used instead of conjugates. A fluorescence spectra for each sample was taken on Dual-FL fluorometer equipped with a Model 350B Temperature Controller set at 20°C (Figure 4.1a). A standard curve of the WT standards was made from integrating the florescence spectra from 300 nm to 385 nm (Figure 4.1b). Once the curve was made, the conjugate samples were integrated, and the protein concentrations were found using the equation from the standard curve. This process was repeated with every set of conjugates to ensure proper concentration determination.

4.2.5 Conjugate Activity

Conjugate activity was run using the same method described in *2.2.2 Activity of Free Mutants*; however, instead of using free protein, conjugates were used. The turnovers were adjusted using the protein concentration obtained from the concentration determination assay.

4.2.6 DHFR to AuNP Conjugates

DHFR:AuNP ratios were deduced from determining the concentration of AuNP and DHFR. The DHFR concentration from the concentration determination assay was ratioed with the AuNP concentration from UV/Vis.

4.3 Results and Discussion

4.3.1 UV/Vis Verification

UV/Vis spectroscopy was used to determine if protein was bound to the AuNP by redshifts in the SPR λ_{max} absorbance of the AuNPs. The free AuNP had a SPR λ_{max} absorbance at 519 nm while the conjugates had a SPR λ_{max} absorbance at 525 nm. The SPR λ_{max} absorbance showed the same shift for conjugates for 5 nm, 15 nm and 30 nm AuNP (Figure 4.1). The SPR λ_{max} absorbance shift occurs because the dielectric constant of the conjugated protein is different from that of the bound citrate on the free AuNPs.

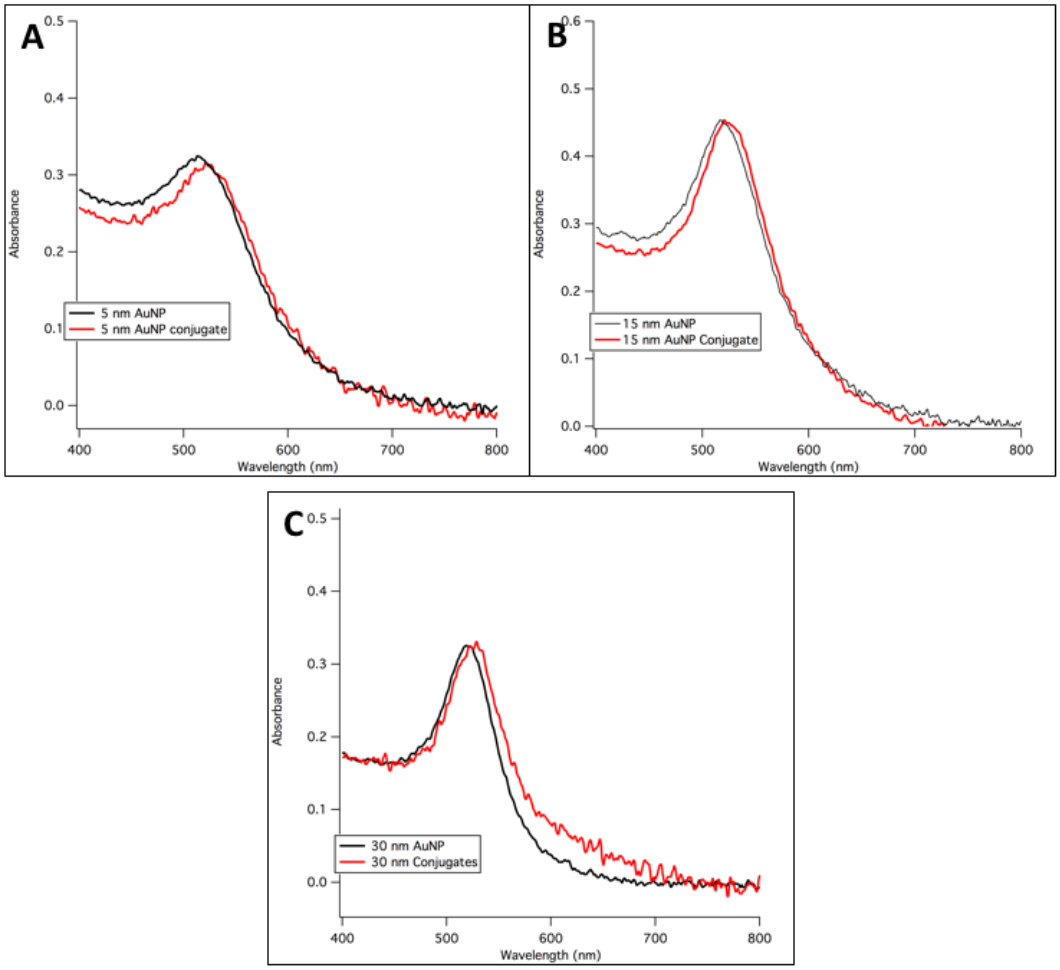

Figure 4.1: UV/Vis comparison of free AuNP and conjugates. **A:** UV/Vis comparison for 5 nm free AuNP and conjugates. **B:** UV/Vis comparison for 15 nm free AuNP and conjugates. **C:** UV/Vis comparison for 30 nm free AuNP and conjugates.

4.3.2 SDS-PAGE

Once the conjugates were made, they had a dark pink to red color depending on the concentration. However, visually inspecting the solution cannot accurately determine if protein has bound to the AuNPs. One method of determining conjugation is to run an SDS-PAGE gel. Free AuNPs do not run through an SDS-PAGE gel and, instead, they precipitate out of solution due to their lack of stabilization (Figure 4.2 Lane 5 and 6, Figure 4.3 Lane 5). On the other hand, when protein is bound to the AuNP, the conjugates move through the SDS Page gel.

When comparing the different size AuNPs in the gel, it is clear that the 5 nm AuNP conjugates moved further than the 15 nm and 30 nm conjugates. This makes sense because the 5 nm conjugates are lighter than the. Even though the 30 nm AuNP conjugates seem to have stayed in the well, however a different gel composition may have allowed the 30-nm conjugate to move. However, the color of the conjugates when compared to color of the black free AuNPs in the well is sufficient enough in determining that the protein is bound to the AuNP.

When a gel with conjugates was destained, it is clear that he preparation is successful because no free protein could be found the a stained. Figure 4.4 shows a stained gel for 15 nm and 30 nm conjugates. Since 5 nm conjugates are performed in a similar manner, it is fair to assume that the 5 nm conjugates also lack free protein.

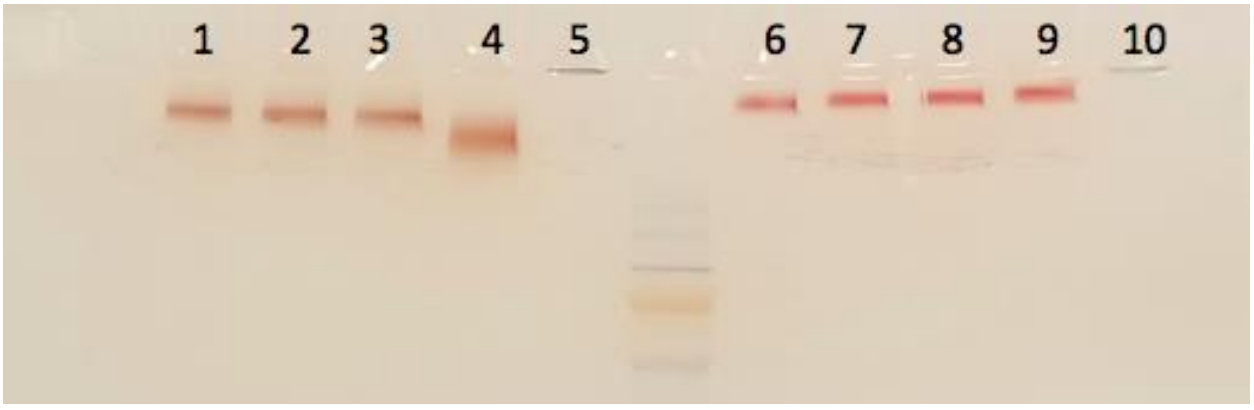

Figure 4.2. SDS-PAGE gel of 5 nm AuNP (lanes 1-5) and 15 nm AuNP (lanes 6-10) conjugates. Lane 1: FG Loop Mutant-5 nm; Lanes 2: Alpha Helix Mutant-5 nm AuNP; Lane 3: Distal Active Site Mutant-5 nm AuNP; Lane 4: AuNP-His-Tag Mutant-5 nm AuNP. Lane 5: Free 5 nm AuNP. Lane 6: FG Loop Mutant-15 nm AuNP; Lane 7: Alpha Helix Mutant-15 nm AuNP; Lane 8: Distal Active Site Mutant-15 nm AuNP; Lane 9: His-Tag Mutant-15 nm AuNP. Lane 10: Free 15 nm AuNP.

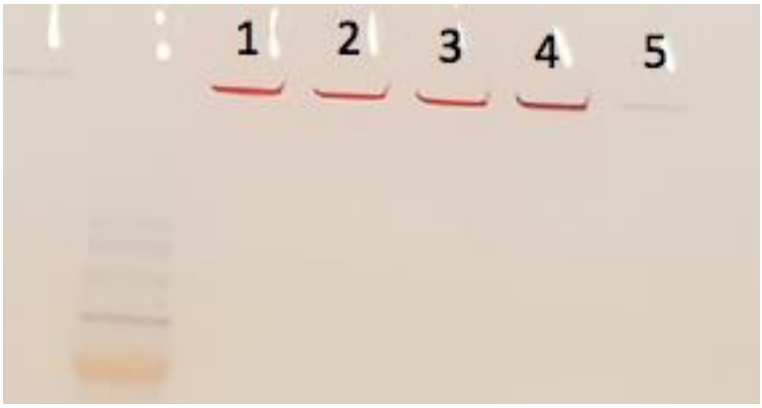

Figure 4.3. SDS-PAGE gel of 30 nm AuNP conjugates. Lane 1: FG Loop Mutant; Lanes 2: Alpha Helix Mutant-30 nm AuNP; Lane 3: Distal Active Site Mutant-30 nm AuNP; Lane 4: His-Tag Mutant-30 nm AuNP. Lane 5: Free 30 nm AuNP.

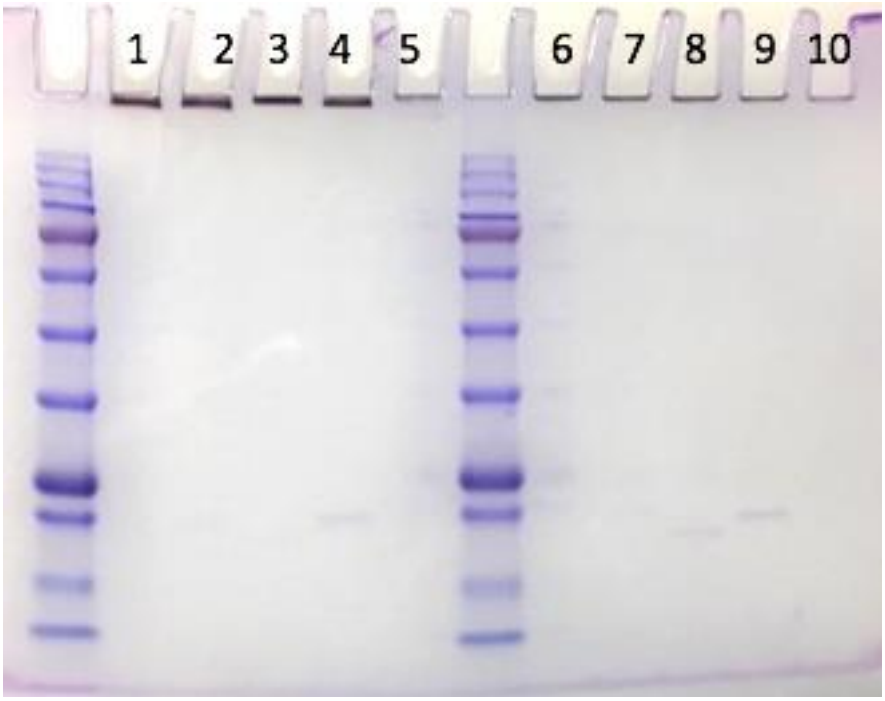

Figure 4.4. Stained SDS-PAGE gel of 15 nm AuNP (lanes 1-5) and 30 nm AuNP (lanes 6-10) conjugates. Lane 1: FG Loop Mutant-15 nm; Lanes 2: Alpha Helix Mutant-15 nm AuNP; Lane 3: Distal Active Site Mutant-15 nm AuNP; Lane 4: His-Tag Mutant-15 nm AuNP. Lane 5: Free 15 nm AuNP. Lane 6: FG Loop Mutant-30 nm AuNP; Lane 7: Alpha Helix Mutant-30 nm

AuNP; Lane 8: Distal Active Site Mutant-30 nm AuNP; Lane 9: His-Tag Mutant-30 nm AuNP. Lane 10: Free 30 nm AuNP.

4.3.3 Dynamic Light Scattering

From the DLS, it was determined that there is a monolayer of enzymes forming about the AuNPs. The purpose of running DLS is to determine the size of the conjugates in comparison to the free AuNP. By looking at the size and diffusion rates obtained from the DLS, it would be possible to see if a monolayer or multilayer of protein is bound to the AuNPs. Knowing the hydrodynamic diameter would allow us to deduce how many layers of protein are present. This analysis was completed with the 15 nm and 30 nm conjugates. The 5 nm conjugates were too small to be detected, and thus are not included in the analysis because DLS only a lower bound limit of approximately 10 nm. The DLS shows that the conjugates are approximately 32 nm in diameter for 15 nm AuNP conjugates and 44 nm for 30 nm AuNP conjugates. The free AuNPs had hydrodynamic diameters of 18 and 34 nm for the free 15 nm and 30 nm free AuNPs. These hydrodynamic diameters are slightly larger than the actually diameters because of water that binds to the spherical object causing the nanosphere to appear approximately 2-3 nanometers longer than it should. Since DHFR is 4 nm by 2 nm,[17] an addition of 8 nm to the diameter of the free AuNP is indicative of a monolayer forming. Since the hydrodynamic diameters are only a few nanometers longer, instead of 16-nm double, it can be concluded that a monolayer of protein, instead of a multilayer, has formed around the AuNPs.

Since DLS measures the diffusion of rate of molecules, faster diffusion is observed when the molecules are smaller, hence in both 15 nm and 30 nm AuNP data sets, the free AuNPs have faster diffusion times when compared to that of the conjugates. In the autocorrelation function (ACF) vs time graph, the free AuNP have a faster diffusion rate that that of the respective

conjugates (Figure 4.5a,c) . The slower diffusion rate of conjugates is indicative that protein has adequately bound to the AuNPs. Furthermore, intensity distributions show that the conjugates have an increase in diameter when compared to the respective free AuNP (Figure 4.5 b,d).

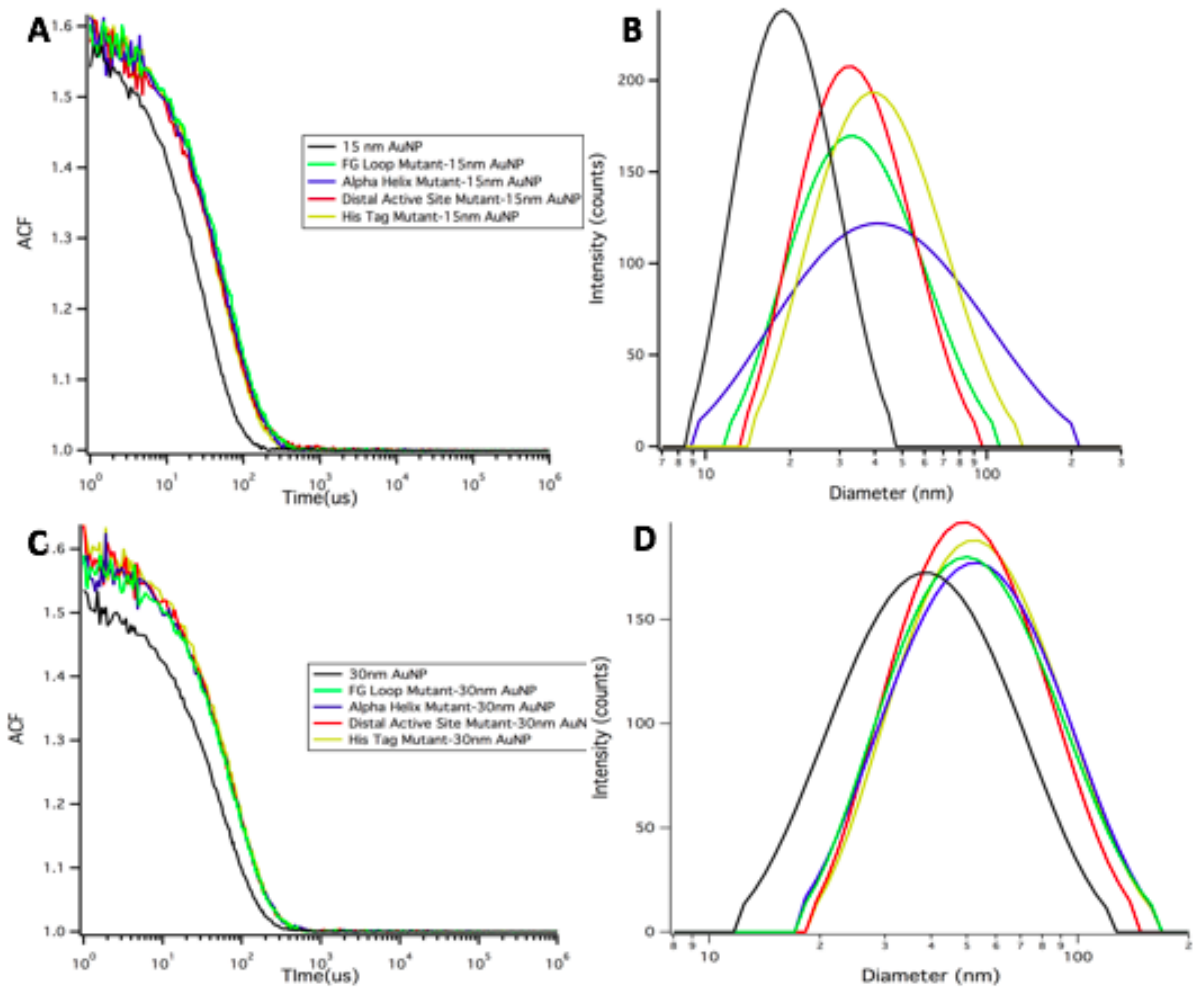

Figure 4.5 A: DLS data for 15 nm AuNP conjugates. **B:** Intensity distributions for 15 nm AuNP conjugates **C:** DLS data for 30 nm AuNP conjugates. **D:** Intensity distributions for 30 nm AuNP conjugates

4.3.4 Concentration Determination

The concentration determination assay was able to adequately determine concentration of DHFR mutants bound to AuNPs. A novel concentration determination assay had to be developed Figure 4.6) because UV/Vis is could not determine concentration at such low concentration with scattering from AuNPs at 280 nm, and Bradford assays could not be performed due to the KCN causing the Bradford dye to degrade. Over many preparations, the range of the concentrations of the enzymes bound to AuNPs were consistent. The assay determined consistently between 2-5 μM of protein bound to the 5 nm AuNPs in multiple preparations. For 15 nm AuNP conjugates, there was 2-4 μM of protein bound, and there was approximately 2-5 μM of protein bound to the 30 nm AuNP conjugates.

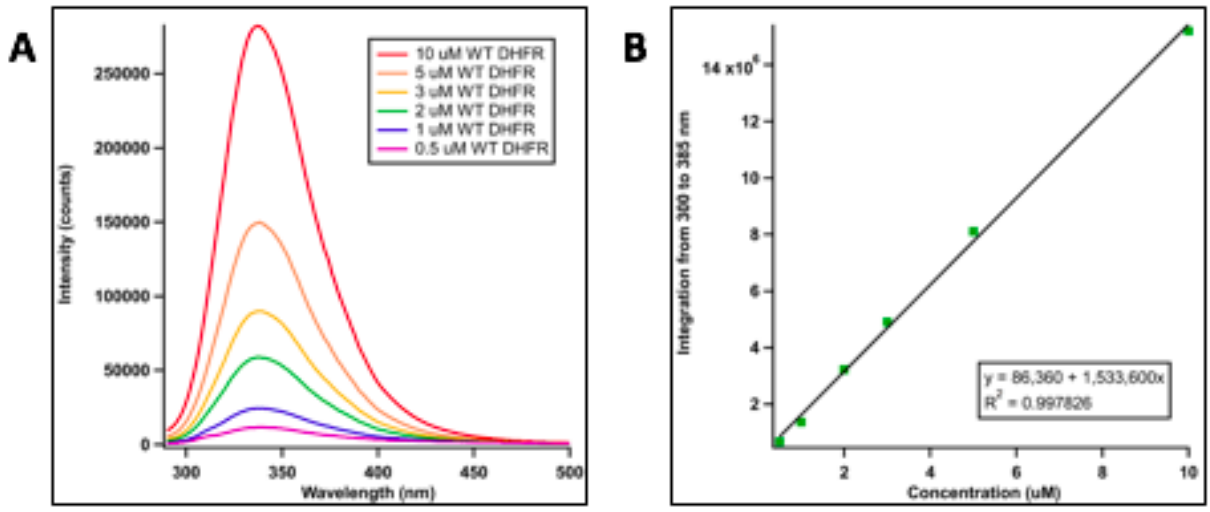

Figure 4.6 A: Fluorescence spectra of WT standards. **B:** Standard curve created by concentration standards on the fluorometer. Reproduced from reference 17.

4.3.5 Conjugate Activity

When comparing the activity of the conjugates with different AuNP sizes to each other, the size of the AuNP did not impact the turnover (Table 4.1). The His-Tag and Alpha Helix mutant conjugates show no difference in activity when the size of the AuNPs were varied. The Distal

Active Site mutant conjugates consistently had higher activity than the other single cysteine mutant conjugates, which is most likely due to the site-specific binding of the AuNP since it is furthest away from the active site. The FG Loop Mutant conjugates showed varied activity, where the activity was not consistent when the size of the AuNPs were varied. The His-Tag conjugates appears to have the same activity regardless of the size of the AuNP, and that is most likely due to the His-Tag association, and possible crowding of the enzyme, which prevents the active site from being exposed. The Alpha Helix mutant conjugates show consistent turnovers throughout varying the AuNP size. The FG Loop mutant conjugates seemed to have the most variation, and this is most likely due to the direct effects of the AuNP on the FG Loop. The Distal Active Site mutant conjugates had greater turnovers than that of the FG Loop and Alpha helix conjugates of similar sizes. This is most likely due to the site-specific binding of the AuNP since it is furthest away from the active site. The Alpha Helix mutant conjugates show consistent turnovers throughout varying the AuNP size. The FG Loop mutant conjugates seemed to have the most variation, and this is most likely due to the direct effects of the AuNP on the FG Loop.

Sample	5 nm AuNP Turnover (s^{-1})	15 nm AuNP Turnover (s^{-1})	30 nm AuNP Turnover (s^{-1})
FG Loop Mutant Conjugates	0.53 +/- 0.1	0.34 +/- 0.3	1.0 +/- 0.2
Alpha Helix Mutant Conjugates	0.3 +/- 0.2	0.38 +/- 0.01	0.4 +/- 0.2
Distal Active Site Mutant Conjugates	0.7 +/- 0.4	0.70 +/- 0.02	1.5 +/- 0.3
His-Tag Mutant Conjugates	0.30 +/- 0.08	0.4 +/- 0.1	0.33 +/- 0.06

Table 4.1. Activity of DHFR-AuNP conjugates (n=3).

4.2.6 DHFR to AuNP Ratios

Since the AuNPs have different diameters of 5 nm, 15 nm and 30 nm, intuitively, they would have increasing surface areas. As the surface area of an AuNP increases, more enzymes can be conjugated. From a simple calculation of the ratio of the surface area of the AuNP to the surface area of DHFR which was approximately 8 nm^2, it was determined that the approximate number of enzymes that could be bound to the AuNPs is 7.8, 70.6 and 283 for the 5 nm, 15 nm and 30 nm AuNP conjugates, respectively. Using concentrations from UV/Vis for the concentration of AuNPs and concentrations from the aforementioned concentration determination assay for the concentration of DHFR, ratios were determined (Table 4.2). The actual number of protein bound to the AuNPs is consistent or lower than that of the estimates for the single cysteine mutants, but larger for the His-Tag mutant. This means that we can trust the data because it makes theoretical sense for the single cysteine mutants because the amount of protein bound is near or below the theoretical maximum. The His-Tag mutant is most likely higher than the theoretical maximum because the His-Tag attachment is longer than that of the single cysteines, meaning that more enzymes could possibly fit around an AuNP. The data shows that the FG Loop, Alpha Helix and Distal Active Site mutants have similar numbers of DHFR attached to the respective AuNP. Approximately 8, 35, and 180 of the single cysteine mutants were bound to the 5, 15 and 30 nm AuNP (Table 4.2). The His-Tag mutant consistently has about twice as much enzyme bound to the respective AuNP and is mostly likely due to the method of attachment which is through a strong association of the His-Tag to the AuNP. The greater number of His-Tag mutants bound to the AuNPs essentially supports the possibility that the low activity for the His-Tag conjugates may be due to overcrowding of enzymes on the AuNPs.

Mutant	DHFR:5 nm AuNP	DHFR:15 nm AuNP	DHFR:30 nm AuNP
FG Loop Mutant Conjugates	8.0	34	179
Alpha Helix Mutant Conjugates	9.2	34	191
Distal Active Site Mutant Conjugates	9.5	35	180
His-Tag Mutant Conjugates	18.4	68	468

Table 4.2. Ratio of DHFR Mutant to 5 nm, 15 nm and 30 nm AuNP post-conjugation. Values were determined from making a ratio of DHFR mutants and AuNPs using concentrations determined from UV/Vis (n=2).

Part V: Conclusion

5. Conclusions

This thesis was aimed to characterize DHFR conjugates with the site-specific conjugation of 5 nm, 15 nm and 30 nm AuNPs. There is not much literature on comparing conjugates in which AuNPs are attached to various sites on an enzyme, even though enzyme conjugation is heavily studied. Conjugation is important for biocatalysts, bio-sensing, biofuels cells, disease diagnosis, and drug delivery, and perhaps one day this information can be used for advancements of these technologies.

The initial characterization of the free enzymes was shown in Part II through the TEV cleavage process, activity and Arrhenius information, which demonstrates that the free mutants maintain similar characteristics to that of the WT. The thesis also presented a method of creating DHFR-AuNP conjugates for 5 nm, 15 nm and 30 nm AuNPs, and showed the process in which Tween 20 was shown to stabilize the conjugates for long-term use throughout the experiments. In Part IV, a novel fluorescence assay was shown to determine the concentration of enzyme conjugated to AuNPs. The UV/Vis data shows that the protein was bound to the conjugates due to the SPR λ_{max} red shifted from 519 nm to 525 nm. SDS-PAGE gels also showed that the protein was bound to the AuNPs and that there was no free protein in the solution. The DLS showed that there was a monolayer of protein on the AuNPs. However, when running the ratios of bound protein to AuNP, the His-Tag mutant consistently showed approximately twice as much protein bound than the other conjugates, this excess could be due method of attachment of the His-Tag mutant on the AuNP because there is a longer chain of histidines in comparison to one rigid cysteine.

Using this information, plenty of future investigations can occur. Heat flow experiments could be done to determine how site-specific heating effects enzyme activity. This can be done with a 527-nm (green) laser, which is removed from most biological absorbances. Likewise, experiments in which AuNPs are used to deliver DHFR to specific sites in an organism's body to potentially augment thymidylate synthesis can also be conducted.

However, to improve this specific investigation, the effect of different linkers can be used to determine how proximity an enzyme to the AuNP affects activity. It is very possible that the low turnovers that were viewed with the conjugates were due to the proximity to the AuNP. After an experiment of this nature is preformed, we can determine how feasible attaching enzymes to AuNP is in order to have future health benefits, since having a direct attachment slows down DHFR activity. Nevertheless, the study at hand provided important advances because it demonstrated the possibility of site-specific binding of DHFR to AuNPs. Overall, viewing site specific attachment of gold nanoparticles at different locations on an enzyme can help us understand the kinetics and dynamics of enzymes and further the relevance of bioconjugation of AuNPs.

Part 6: References

References

(1) R.; Lillard, J. W. *Experimental and Molecular Pathology* **2009**, *86* (3), 215–223.

(2) Freestone, I.; Meeks, N.; Sax, M.; Higgitt, C. *Gold Bulletin* **2007**, *40* (4), 270–277.

(3) Hansen, D. *Leonardo* **2011**, *44* (2), 166–167.

(4) Schoemaker, H. E. *Science* **2003**, *299* (5613), 1694–1697.

(5) Demin, S.; Hall, E. A. *Bioelectrochemistry* **2009**, *76* (1-2), 19–27.

(6) Arruda, D. L.; Wilson, W. C.; Nguyen, C.; Yao, Q. W.; Caiazzo, R. J.; Talpasanu, I.; Dow, D. E.; Liu, B. C.-S. *Expert Review of Molecular Diagnostics* **2009**, *9* (7), 749–755.

(7) Lata, J. P.; Gao, L.; Mukai, C.; Cohen, R.; Nelson, J. L.; Anguish, L.; Coonrod, S.; Travis, A. J. *Bioconjugate Chemistry* **2015**, *26* (9), 1931–1938.

(8) Ghosh, S. K.; Pal, T. *Chemical Reviews* **2007**, *107* (11), 4797–4862.

(9) Blankschien, M. D.; Pretzer, L. A.; Huschka, R.; Halas, N. J.; Gonzalez, R.; Wong, M. S. *ACS Nano* **2012**, *7* (1), 654–663.

(10) Govorov, A. O.; Richardson, H. H. *Nano Today* **2007**, *2*, 30.

(11) Fierke, C. A.; Johnson, K. A.; Benkovic, S. J. *Biochemistry* **1987**, *26*, 4085.

(12) Oyeyemia, O. A.; Sours, K. M.; Leeb, T.; Resing, K. A.; Ahnb, N. G.; Klinman, J. P. *Proc. Natl. Acad. Sci. (USA)* **2010**, *107*, 10074.

(13) Hammes-Schiffer, S. *Current Opinion in Structural Biology* **2004**, *14* (2), 192–201.

(14) Sawaya, M. R.; Kraut, J. *Biochemistry* **1997**, *36*, 586

(15) Mcelheny, D.; Schnell, J. R.; Lansing, J. C.; Dyson, H. J.; Wright, P. E. *Proceedings of the National Academy of Sciences* **2005**, *102* (14), 5032–5037.

(16) Boehr, D. D.; McElheny, D.; Dyson, H. J.; Wright, P. E. *Science* **2006**, *313*, 1638.

(17) Kozlowski, R.; Ragupathi, A.; Dyer, R. B.; *Bioconjugate Chemistry*, In preperation

(18) Venkitakrishnan, R. P.; Zaborowski, E.; Mcelheny, D.; Benkovic, S. J.; Dyson, H. J.; Wright, P. E. *Biochemistry* **2005**, *44* (15), 5948–5948.

(19) Ames, B. N.; Shigenaga, M. K.; Park, E.-M. *Oxidative Damage & Repair* **1991**, 181–187.

(20) Rajagopalan, P. T. R.; Zhang, Z.; Mccourt, L.; Dwyer, M.; Benkovic, S. J.; Hammes, G. G. *Proceedings of the National Academy of Sciences* **2002**, *99* (21), 13481–13486.

(21) Brogden, R.; Carmine, A.; Heel, R.; Speight, T.; Avery, G. *Drugs* **1982**, *23* (6), 405–430.

(22) Zhao, Y.; Zhou, F.; Zhou, H.; Su, H. *Phys. Chem. Chem. Phys.* **2013**, *15* (5), 1690–1698.

(23) Pensa, E.; Cortés, E.; Corthey, G.; Carro, P.; Vericat, C.; Fonticelli, M. H.; Benítez, G.; Rubert, A. A.; Salvarezza, R. C. *Accounts of Chemical Research* **2012**, *45*, 1183.

(24) Singh, P.; Francis, K.; Kohen, A. *ACS Catalysis* **2015**, *5* (5), 3067–3073.

(25) Krögera, D.; Liley, M.; Schiweck, W.; Skerra, A.; Vogel, H. *Biosensors and Bioelectronics* **1999**, *14* (2), 155–161.

(26) Tada, H.; Soejima, T.; Ito, S.; Kobayashi, H. *Journal of the American Chemical Society* **2004**, *126* (49), 15952–15953.

(27) Hainfeld, J. F.; Liu, W.; Halsey, C. M.; Freimuth, P.; Powell, R. D. *Journal of Structural Biology* **1999**, *127* (2), 185–198.

(28) Stols, L.; Gu, M.; Dieckman, L.; Raffen, R.; Collart, F. R.; Donnelly, M. I. *Protein Expression and Purification* **2002**, *25* (1), 8–15.

(29) Heidary, D. K.; O'neill, J. C.; Roy, M.; Jennings, P. A. *Proceedings of the National Academy of Sciences* **2000**, *97* (11), 5866–5870.

(30) Cline, D. J.; Redding, S. E.; Brohawn, S. G.; Psathas, J. N.; Schneider, J. P.; Thorpe, C.*Biochemistry* **2004**, *43* (48), 15195–15203.

(31) Fruscione, F.; Sturla, L.; Duncan, G.; Etten, J. L. V.; Valbuzzi, P.; Flora, A. D.; Zanni, E. D.; Tonetti, M. *Journal of Biological Chemistry* **2007**, *283* (1), 184–193.

(32) Kuriyan, J.; Konforti, B.; Wemmer, D. *The molecules of life: physical and chemical principles*; Garland Science: New York, 2012.

(33) Liu, X.; Atwater, M.; Wang, J.; Huo, Q. *Colloids and Surfaces B: Biointerfaces* **2007**, *58*(1), 3–7.

(34) Tong, W.; Sprules, T.; Gehring, K.; Saragovi, H. U. *Rational Drug Design* **2012**, 39–52.

(35) Yehl, K.; Joshi, J. P.; Greene, B. L.; Dyer, R. B.; Nahta, R.; Salaita, K. *ACS Nano* **2012**, *6*(10), 9150–9157.

(36) Hochuli, E. *Genetic Engineering* **1990**, 87–98.

(37) Chrétien, A.; Gagnon-Arsenault, I.; Dubé, A. K.; Barbeau, X.; Després, P. C.; Lamothe, C.; Dion-Côté, A.; Lagüe, P.; Landry, C. R. *Molecular & Cellular Proteomics* **2017**, *17* (2), 373–383.

(38) Hill, H. D.; Mirkin, C. A. *Nature Protocols* **2006**, *1* (1), 324–336.

(39) Giannuzzi, L.; Stevie, F. *Micron* **1999**, *30* (3), 197–204.

(40) Ditzler, L. R.; Sen, A.; Gannon, M. J.; Kohen, A.; Tivanski, A. V. *Journal of the American Chemical Society* **2011**, *133* (34), 13284–13287.